Therefore, the important point emerging from this work is that, within wide limits, the level of acidity of the medium is the principal determinant of cation speciation, regardless of whether oxidant or reductant is in excess. This certainly holds when the disproportionation reactions are reversed. The generalization would not be valid if F_2 were to be in excess. Its extreme power as an oxidant would override solution acidity/basicity effects.

A further indication of the prime importance of acidity control in generating individual cations was that conproportionation reactions similar to those described above for IF_5 and I_2 were carried out within the present study with IO_3^- and I_2 in HF solutions of controlled acidity. SbF_5 gave I_2^+, and GeF_4, potentially a Lewis acid of the system but one that is almost vanishingly weak, gave I_5^+ and I_3^+. This, however, is an untidy way of producing cations by comparison with the reaction of IF_5 and I_2, because each of the oxo ligands of IO_3^- would be triply protonated in HF on release from the oxidant, generating much of the unnecessary base F^-. However, this approach could be used for convenience in the synthesis of iodine cations. We have shown this to be a general synthetic approach by generating sulfur cations by reaction of S_8 with SO_3^{2-} and with SO_4^{2-} in HF, the acidity of which has been adjusted appropriately.

The overall program on generation of individual cations by control of the HF acidity is summarized briefly in the flow sheet in Figure 5. Excess reductant, I_2, with F_2 gives I_5^+ and I_3^+ for H_0 values between −11 and −16.2 and I_2^+ in more acidic solutions. Each cation disproportionates to I_2 and IF_5 when treated in solution with excess base. With the disproportionation products in solution and, now, the oxidant in excess, appropriate acidity control leads to generation in solution of I_5^+, I_3^+, or I_2^+.

This scheme is presented to highlight the proposition developed in this paper that the principal determinant of the nature of cations of iodine stabilized in AHF is the level of acidity or basicity of the solution.

Acknowledgment. We wish to acknowledge substantial financial support from the Australian Research Grants Scheme, which provided the salary of J.B. as well as the cost of expensive maintenance items.

Registry No. SbF_5, 7783-70-2; NbF_5, 7783-68-8; TaF_5, 7783-71-3; HF, 7664-39-3; F_2, 7782-41-4; NaF, 7681-49-4; NaCl, 7647-14-5; I_2, 7553-56-2; IF_5, 7783-66-6; I_3^+, 12596-32-6; I_5^+, 44222-71-1; I_2^+, 28712-14-3.

Contribution from the Departments of Chemistry, University of Tennessee, Knoxville, Tennessee 37996-1600, and The University of North Carolina at Charlotte, Charlotte, North Carolina 28223

ESR Study of the Solution Thermochromism Resulting from Low-Temperature Isomerization of Pyrazolato-Bridged Dirhodium Complexes Generated via Electrochemical Oxidation

Clifton Woods,*,† Louis J. Tortorelli,† D. Paul Rillema,‡ James L. E. Burn,† and Jeffrey C. DePriest†

Received May 5, 1988

Paramagnetic complexes of the type $[Rh_2(\mu\text{-}EE')_2(t\text{-}BuNC)_2(\mu\text{-}Z)](PF_6)_2$ (EE′ = bis(diphenylphosphino)methane (dppm), (diphenylarsino)(diphenylphosphino)methane (dapm), bis(diphenylarsino)methane (dpam); Z = pyrazolate (pz), 4-methylpyrazolate (4mpz), 3,5-dimethylpyrazolate (35mpz), 4-bromo-3,5-dimethylpyrazolate (4B35mpz), 3,4,5-tribromopyrazolate (345Bpz)) containing the Rh_2^{3+} core have been prepared via controlled-potential electrolysis of the parent Rh_2^{2+} species $[Rh_2(\mu\text{-}EE')_2(t\text{-}BuNC)_2(\mu\text{-}Z)](PF_6)$. The Rh_2^{2+} diisocyanide complexes and analogous dicarbonyl complexes have cyclic voltammograms that exhibit a quasi-reversible wave followed by an irreversible or a second quasi-reversible wave. The $E_{1/2}$ values for the couple at less positive potentials are in the order dppm < dapm < dpam for analogous diisocyanide and dicarbonyl complexes; thus, the stabilities of the Rh_2^{3+} paramagnetic complexes toward reduction are in the order dpam < dapm < dppm. UV–vis spectroscopy has been used to demonstrate that electron transfer occurs between Rh_2^{2+} and Rh_2^{3+} species containing different EE′ ligands when the initial Rh_2^{3+} species is the less stable one of the two possible Rh_2^{3+} species. Solutions of the Rh_2^{3+} diisocyanide species in 4:1 CH_2Cl_2/toluene at room-temperature are green and give room-temperature ESR spectra that exhibit a single isotropic signal near $g = 2.15$. The frozen solutions exhibit anisotropic ESR spectra with resonances between g values of 1.99 and 2.22. Frozen solutions of the Rh_2^{3+} diisocyanide species at −196 °C are red, except for $[Rh_2(\mu\text{-dppm})_2(t\text{-}BuNC)_2(\mu\text{-}345Bpz)](PF_6)_2$, which remains green. Frozen-solution spectra at temperatures above −196 °C for $[Rh_2(\mu\text{-dapm})_2(t\text{-}BuNC)_2(\mu\text{-}345Bpz)](PF_6)_2$ clearly indicate the existence of two forms of the complex, a green α form and a red β form. The temperatures at which the α to β isomerization occurs are in the order dppm < dapm < dpam for a given pyrazolate. The possible nature of this isomerization is discussed.

Introduction

In recent years a very rich chemistry has been discovered for dirhodium complexes containing bis(diphenylphosphino)methane (dppm)[1] and, to a lesser extent, (diphenylarsino)(diphenylphosphino)methane (dapm) and bis(diphenylarsino)methane (dpam) as transoid bridging ligands. Unlike the dirhodium tetracarboxylate complexes $Rh_2(O_2CR)_4$ and analogous complexes that contain the Rh_2^{4+} core and four anionic bridging ligands,[2,3] the majority of the known dirhodium complexes with transoid dppm, dapm, and dpam ligands contain the Rh_2^{2+} core. A few dirhodium(II) complexes containing the transoid dppm, dapm, and dpam ligands have been prepared by either chemical or electrochemical oxidative addition.[4-7]

Many of the Rh_2^{4+} complexes with four anionic ligands have been shown to undergo electrochemical oxidation to form Rh_2^{5+}

* To whom correspondence should be addressed.
† University of Tennessee.
‡ The University of North Carolina at Charlotte.

(1) (a) Balch, A. L. In *Homogeneous Catalysis with Metal Phosphine Complexes*; Pignolet, L. G., Ed.; Plenum: New York, 1984; Chapter 5. (b) Sanger, A. R. *Ibid.*; Chapter 6.
(2) (a) Cotton, F. A.; Walton, R. A. *Multiple Bonds Between Metal Atoms*; Wiley-Interscience: New York, 1982; p 311. (b) Felthouse, T. R. *Prog. Inorg. Chem.* **1982**, *20*, 109. (c) Berry, M.; Garner, C. D.; Hillier, I. H.; Macdowell, A. A.; Clegg, W. *J. Chem. Soc., Chem. Commun.* **1980**, 494. (d) Cotton, F. A.; Felthouse, T. R. *Inorg. Chem.* **1981**, *20*, 584. (e) Boyer, E. B.; Robinson, S. D. *Coord. Chem. Rev.* **1983**, *50*, 109. (f) Tocher, D. A.; Tocher, J. H. *Inorg. Chim. Acta* **1985**, *104*, L15. (g) Duncan, J.; Malinski, T.; Zhu, T. P.; Hu, Z. S.; Kadish, K. M. *J. Am. Chem. Soc.* **1982**, *103*, 5507. (h) Barron, A. R.; Wilkinson, G.; Motevalli, M.; Hursthouse, M. B. *Polyhedron* **1985**, *4*, 1131.
(3) Le, J. C.; Chavan, M. Y.; Chau, L. K.; Bear, J. L.; Kadish, K. M. *J. Am. Chem. Soc.* **1985**, *107*, 7195.
(4) (a) Balch, A. L.; Tulyanthan, B. *Inorg. Chem.* **1977**, *16*, 2840. (b) Balch, A. L.; Labadie, J. W.; Delker, G. *Inorg. Chem.* **1979**, *18*, 1224. (c) Balch, A. L. *J. Am. Chem. Soc.* **1976**, *98*, 8049.

0020-1669/89/1328-1673$01.50/0

Table I. Pyrazolato-Bridged Dirhodium Compounds of the General Formula $[Rh_2(\mu\text{-}EE')_2(\mu\text{-}Z)L_2]PF_6$[a]

no.	EE′	Z	L	no.	EE′	Z	L
1	dppm	pz	RNC	16	dapm	pz	CO
2	dppm	4mpz	RNC	17	dapm	4mpz	CO
3	dppm	35mpz	RNC	18	dapm	35mpz	CO
4	dppm	4B35mpz	RNC	19	dapm	4B35mpz	CO
5	dppm	345Bpz	RNC	20	dapm	345Bpz	CO
6	dppm	pz	CO	21	dpam	pz	RNC
7	dppm	4mpz	CO	22	dpam	4mpz	RNC
8	dppm	35mpz	CO	23	dpam	35mpz	RNC
9	dppm	4B35mpz	CO	24	dpam	4B35mpz	RNC
10	dppm	345Bpz	CO	25	dpam	345Bpz	RNC
11	dapm	pz	RNC	26	dpam	pz	CO
12	dapm	4mpz	RNC	27	dpam	4mpz	CO
13	dapm	35mpz	RNC	28	dpam	35mpz	CO
14	dapm	4B35mpz	RNC	29	dpam	4B35mpz	CO
15	dapm	345Bpz	RNC	30	dpam	345Bpz	CO

[a] EE′ = dppm, dapm, dpam; Z = pyrazolate (pz), 4-methylpyrazolate (4mpz), 3,5-dimethylpyrazolate (35mpz), 4-bromo-3,5-dimethylpyrazolate (4B35mpz), 3,4,5-tribromopyrazolate, (345Bpz); RNC = $(CH_3)_3CNC$.

complexes.[8] It has also been shown that a few of these Rh_2^{4+} complexes can be reduced to form stable complexes with the Rh_2^{3+} core.[3,9] Recently a related complex with the Rh^{3+} core has been generated from one with a Rh^{2+} core via electrochemical oxidation.[10] Due to the interest in dirhodium complexes and the lack of data on the electrochemical properties of dirhodium(I) complexes containing the dppm, dapm, and dpam ligands, we began an investigation of the potentially rich electrochemistry of these complexes.[6,11,12]

One class of compounds that has been of particular interest to us is the A-frame dirhodium complexes of structure I that contain

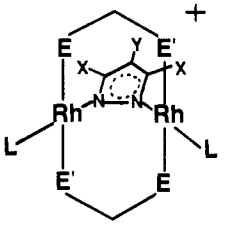

I

pyrazolate anions in the apex position and dppm, dapm, or dpam as the transoid bridging ligands. The synthesis and the structural and spectroscopic characterization of these complexes have been reported.[5,6] Herein we report results of some electrochemical and ESR studies of complexes of structure I. The complexes discussed in this paper are listed in Table I.

Experimental Section

Materials. The procedures used for the preparation of the dirhodium complexes listed in Table I have been previously reported.[6] Pyrazole (Hpz), 4-methylpyrazole (H4mpz), and 3,5-dimethylpyrazole (H35mpz) were purchased from Aldrich Chemicals. 4-Bromo-3,5-dimethylpyrazole (H4B35mpz) was obtained from Pfaltz and Bauer, and 3,4,5-tribromopyrazole (H345Bpz) was prepared by literature procedures.[13] Dichloromethane was dried over anhydrous $CaCl_2$ and freshly distilled under Ar from P_2O_5 just prior to use.[14] Methanol was distilled and degassed with Ar immediately before use.

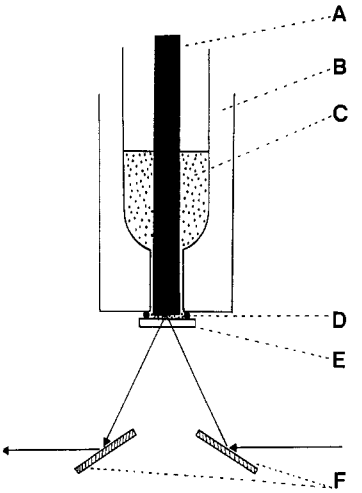

Figure 1. Drawing of the infrared spectroelectrochemistry cell. Labeled parts: (A) platinum button electrode; (B) coolant compartment; (C) electrolysis solution; (D) O-ring; (E) KBr disk; (F) gold-surfaced planar mirrors.

Physical Measurements. UV–vis spectra were recorded on a Cary 219 spectrophotometer. Routine infrared (IR) spectra between 4000 and 400 cm^{-1} were obtained on a Perkin Elmer 1330 spectrophotometer. The samples were prepared as Nujol mulls sealed between polyethylene sheets. Near-IR spectra were obtained between 800 and 2200 nm on a Cary 17D spectrophotometer. UV–vis and near-IR spectra were recorded by using 1.0 cm quartz cells with degassed CH_2Cl_2 as the solvent. All ESR spectra were obtained on 4:1 CH_2Cl_2/toluene solutions with a JEOL JES-PE-IX ESR spectrometer. Spectra at −196 °C were obtained by using a liquid-N_2 Dewar and frozen-solution spectra at temperatures above −196 °C were recorded by using a variable-temperature accessory.

Electrochemistry. Cyclic voltammetry, coulometry, and controlled-potential electrolysis were performed with a BAS-100 electrochemical analyzer (Bioanalytical Systems). The working electrode for voltammetry was a platinum-button electrode (Beckman) with a surface area of 0.24 cm^2. The electrode surface was polished with 0.3-μm polishing alumina prior to each run. The auxiliary electrode was a 2.76 cm^2 platinum grid, and the reference electrode was a saturated calomel electrode (SCE). The reference electrode was placed in a glass capillary with a glass frit on one end to separate the reference electrode from the bulk solution. The electrolysis cell was a conventional H-shaped three-compartment cell in which the compartments were separated by glass frits of medium porosity. For electrolysis experiments the working electrode and the auxiliary electrode, a carbon rod, were placed in separate outer compartments of the H-cell. The reference electrode was the SCE. All solutions for electrochemical experiments were degassed with Ar or purified N_2. All electrochemical data were obtained at 25 °C and are uncorrected for junction potentials.

Low-Temperature Infrared Spectroelectrochemistry. The cell used for infrared spectroelectrochemistry is diagramed in Figure 1 and consists of a platinum-button working electrode (A), a SCE reference electrode, and a platinum-foil counter electrode housed in an open glass container. The reference and counter electrodes (not shown in Figure 1) were placed in separate glass tubes fitted with glass frits of medium porosity and containing electrolyte solution. The glass tubes were placed in the bulk electrolysis solution (C). This configuration made it possible to isolate the counter and reference electrodes from the bulk solution. A KBr disk (E) (3-cm diameter and 2-cm thickness) was sealed to the bottom of the glass container via an O-ring (D) and served as the infrared window. The glass container with the KBr disk was housed in a metal container with an opening in its bottom to allow the source beam to be reflected onto the KBr window and working electrode.

The potential of the working electrode was controlled by a PAR Model 174A polarographic analyzer in conjunction with a PAR Model 175 universal programmer. Voltammograms were recorded on an Omnigraphic 2000 X-Y recorder (Houston Instruments).

(5) Oro, L. A.; Carmona, D.; Perez, P. L.; Esteban, M.; Tiripicchio, A.; Tiripicchio-Camellini, M. *J. Chem. Soc., Dalton Trans.* **1985**, 973.
(6) Janke, C. J.; Tortorelli, L. J.; Burn, J. L. E.; Tucker, C. A.; Woods, C. *Inorg. Chem.* **1986**, *25*, 4597.
(7) Tortorelli, L. J.; Tinsley, P. W.; Woods, C.; Janke, C. J. *Polyhedron* **1988**, *7*, 315.
(8) (a) Chavan, M. Y.; Zhu, T. P.; Lin, X. Q.; Ahsan, M. Q.; Bear, J. L.; Kadish, K. M. *Inorg. Chem.* **1984**, *23*, 4538. (b) Bear, J. L.; Zhu, T. P.; Malinski, T.; Dennis, A. M.; Kadish, K. M. *Inorg. Chem.* **1984**, *23*, 674. (c) Bear, J. L.; Liu, L.-M.; Kadish, K. M. *Inorg. Chem.* **1987**, *26*, 2927. (d) Chakravarty, A. R.; Cotton, F. A.; Tocher, D. A.; Tocher, J. H. *Inorg. Chim. Acta* **1985**, *101*, 185.
(9) Piranino, P.; Bruno, G.; Loi Schiavo, S.; Laschi, F.; Zannello, P. *Inorg. Chem.* **1987**, *26*, 2205.
(10) Connelly, N. G.; Garcia, G. *J. Chem. Soc., Chem. Commun.* **1987**, 246.
(11) Womack, D. R.; Enlow, P. E.; Woods, C. *Inorg. Chem.* **1983**, *22*, 2653.
(12) Boyd, D. C.; Matsch, P. A.; Mixa, M. M.; Mann, K. R. *Inorg. Chem.* **1986**, *25*, 3333.
(13) *Chem. Abstr.* **1975**, *82*, 112068c.
(14) Gordon, A. J.; Ford, R. A. *The Chemists Companion*; Wiley-Interscience: New York, 1972; p 434.

Table II. Peak Potentials in mV vs SCE for Dirhodium Pyrazolato-Bridged Complexes of the Type $[Rh_2(\mu\text{-}EE')_2(\mu\text{-}Z)L_2]PF_6$[a]

	dppm: E = E′ = P				dapm: E = P; E′ = As				dpam: E = E′ = As			
L	$E_{pl,a}$	$E_{pl,c}$	$E_{p2,a}$	$Ep_{2,c}$	$E_{pl,a}$	$E_{pl,c}$	$E_{p2,a}$	$E_{p2,c}$	$E_{pl,a}$	$E_{pl,c}$	$E_{p2,a}$	$E_{p2,c}$
					Z = Pyrazolate							
CO	816	644	1296	950	857	744	1216	1000	1035	846	1172	
t-BuNC	139	−33	1139	698	189	98	1097	620	278	201	902	625
					Z = 4-Methylpyrazolate							
CO	777	658	1302	927	828	729	1174	950	955	842	1150	
t-BuNC	143	−27	1124	686	168	100			275	200	911	667
					Z = 3,5-Dimethylpyrazolate							
CO	830	641	1480	1050	875	750	1289	1000	920	836	1250	1100
t-BuNC	119	−9	1201	611	203	89	1234		258	183	996	680
					Z = 4-Bromo-3,5-dimethylpyrazolate							
CO	845	715	1431	1080	930	841	1356	1150	997	900	1289	1150
t-BuNC	188	43	1175	698	222	146	1170	700	314	231	902	676
					Z = 3,4,5-Tribromopyrazolate							
CO	923	831	1448	1150	1049	910	1353	1170	1130	845	1271	
t-BuNC	309	146	1150	650	356	257	1320		439	656	1034	760

[a] These data were obtained at 25 °C in CH_2Cl_2 containing 0.10 M TBAH at 100 mV/s and are average values of at least three measurements with a range of ±4 mV.

The infrared spectra were obtained by using a Digilab FTS-20E Fourier transform spectrometer equipped with a high-temperature ceramic source and DTGS detector. The reflectance attachment was constructed in house and consisted of two gold-surfaced planar mirrors (F) held in adjustable aluminum mounts.

A flow of dry nitrogen was maintained above the degassed electrolysis solution (C) throughout the entire experiment. The cell was mounted in a vertical configuration above the spectrometer's sample compartment, and a thin layer of solution (ca. 1–100 μm) was isolated by pressing the working electrode firmly against the KBr window. This sample layer was then sampled via external reflectance as described by Foley et al.[15] IR spectra were obtained at the rest potential and at potentials just past the first and second anodic waves in the cyclic voltammogram of the pyrazolato-bridged dirhodium(I) complexes. Typically, 300–500 IR scans were collected before transformation.

Frozen-solution IR spectra were obtained via reflectance by using the cell shown in Figure 1, with the outer compartment (B) filled with liquid N_2.

Preparation of $[Rh_2(\mu\text{-}EE')_2(t\text{-}BuNC)_2(\mu\text{-}Z)](PF_6)_2$ (EE′ = dppm, dapm, dpam; Z = pz, 4mpz, 35mpz, 4B35mpz, 345Bpz). The appropriate pyrazolato-bridged dirhodium(I) diisocyanide complex (0.10 mmol) in 50 mL of a CH_2Cl_2 solution containing 0.10 M TBAH was oxidized via controlled-potential electrolysis at potentials that were approximately 200–300 mV more positive than the appropriate $E_{1/2}$ values obtained from the data given in Table II by taking the mean of E_{pa} and E_{pc}. The resulting green oxidized solutions were stripped to dryness via a rotary evaporator, and 50 mL of CH_3OH was added. After being stirred overnight, the solutions were filtered to yield green crystalline solids. The products were recrystallized from CH_2Cl_2/ether/hexanes and dried in vacuo. The yields were 70–80%. In the text, these compounds are identified by the number of their parent compounds given in Table I followed by the letter a.

Anal. Calcd for **4a**, $C_{65}H_{68}BrF_{12}N_4P_6Rh_2$: C, 48.65; H, 4.27. Found: C, 48.20; H 4.22. Calcd for **14a**, $C_{65}H_{68}As_2BrF_{12}N_4P_4Rh_2$: C, 46.12; H, 4.05. Found: C, 45.12; H, 4.09. Calcd for **24a**, $C_{65}H_{68}As_4BrF_{12}N_4P_2Rh_2$: C, 43.81; H, 3.84. Found 42.32, H, 3.91.

Results and Discussion

Electrochemistry and Electronic Spectroscopy. The cyclic voltammetric behavior between +1.6 and −1.4 V (vs SCE) of all complexes listed in Table I was recorded at a platinum electrode in CH_2Cl_2, and the data are presented in Table II. The voltammetric behavior of all complexes is similar to that illustrated in Figure 2. The voltammetric behavior consists of a quasi-reversible electron transfer followed at more positive potentials by either an irreversible electron transfer or a second quasi-reversible electron transfer. The potential difference between the two anodic peaks decreases in going from analogous dppm to dapm to dpam complexes such that the voltammograms of some of the dpam complexes exhibit considerable overlap of the two oxidation waves. In those cases where the two oxidation waves are clearly separated,

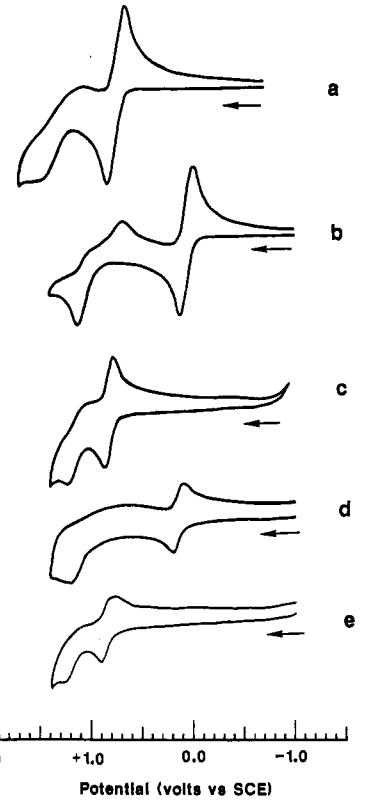

Figure 2. Cyclic voltammograms in CH_2Cl_2/TBAH of (a) **8**, (b) **3**, (c) **18**, (d) **13**, and (e) **28**.

such as with the dppm diisocyanide complexes **1–5**, several diagnostic tests confirm the quasi-reversibility of the first electron transfer on the cyclic time scale. Over the range of scan rates from 50 to 500 mV the i_{pc}/i_{pa} ratio is essentially constant and nearly equal to 1, the current function $i_{pa}/v^{1/2}$ and the $E_{1/2}$ values remain essentially constant, and the ΔE_p values gradually increase.

Controlled-potential coulometry indicates that each oxidation process is a one-electron charge transfer. Thus, the first oxidation process represents the conversion of the parent Rh_2^{2+} species to a Rh_2^{3+} species and the second oxidation process represents the conversion of the Rh_2^{3+} species to a Rh_2^{4+} species. Attempts to isolate a Rh(II)–Rh(II) product generated by controlled-potential electrolysis in CH_2Cl_2/TBAH at potentials just positive of the peak potential of the second oxidation process have been unsuccessful. Our inability to isolate a Rh(II)–Rh(II) species is probably related to the tendency of the d^7 Rh(II) center to acquire a higher

(15) Foley, J. K.; Pons, S. *Anal. Chem.* **1985**, *57*, 945A.

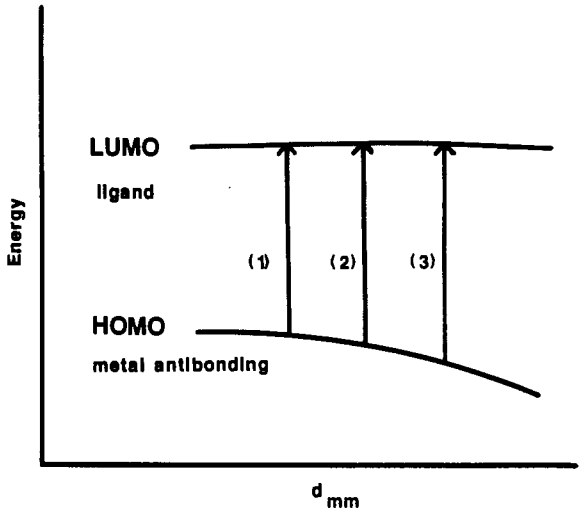

Transition	Complex	d_{mm} (Å)
(1)	E=E'=P	3.060
(2)	E=P; E'=As	(3.140)
(3)	E=E'=As	3.220

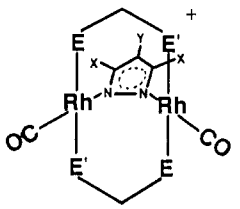

Figure 3. Variation of HOMO–LUMO separation versus Rh···Rh distance for $[Rh_2(\mu\text{-}EE')_2(\mu\text{-}35mpz)(CO)_2]PF_6$ as EE' is changed from dppm to dapm to dpam. The metal–metal distances have been determined for the dppm[5] and the dpam[6] complexes. The metal–metal distance for the dapm complex is approximated by taking the mean of the distances of the dppm and the dapm complexes.

coordination number, but it is unable to do so due to the poor coordinating ability of CH_2Cl_2.

Controlled-potential electrolysis of the diisocyanide complexes at potentials between the two oxidation waves is accompanied by a color change from red or reddish-orange to green and affords a green isolable one-electron-oxidation product for most of the dppm, dapm, and dpam diisocyanide complexes. The dicarbonyl complexes **6–10** can also be oxidized in a one-electron process to afford isolable oxidation products. These one-electron-oxidation products are formally the mixed-valence Rh(I)–Rh(II) complexes and thus are paramagnetic.

The trends observed in the electronic spectral data of the pyrazolato-bridged dirhodium(I) complexes were previously discussed in terms of the orbital picture used to explain the electronic properties of face-to-face rhodium dimers.[5] By analogy to the more descriptive model used by Hoffman and co-workers[16] to discuss the electronic properties of A-frame complexes, the HOMO of the pyrazolato-bridged complexes is likely to be an orbital resulting from the antibonding interaction of two metal orbitals and to have either a_2 or b_2 symmetry. The d^7–d^7 A-frame complexes discussed by Hoffman and co-workers have a b_2 LUMO, suggesting that the HOMO of the formal d^7–d^8 and d^8–d^8 complexes is probably of b_2 symmetry. The model suggests that in A-frame complexes such as the pyrazolato-bridged complexes where the terminal and the apex ligands have antibonding acceptor orbitals, a linear combination of the acceptor orbitals of either the terminal or the apex ligand is likely to be the LUMO. The LUMO for the d^7–d^8 and d^8–d^8 complexes is probably a pyrazolato-based orbital.

(16) Hoffman, D. M.; Hoffman, R. *Inorg. Chem.* **1981**, *20*, 3543.

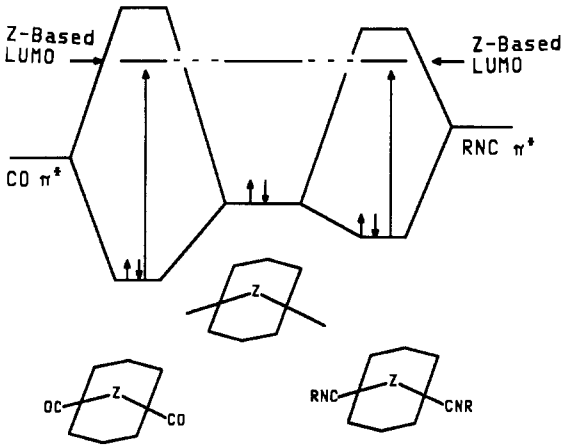

Figure 4. Simple qualitative MO diagram showing the effect of CO versus *t*-BuNC on the HOMO for some pyrazolato-bridged dirhodium complexes.

Table III. Lowest Energy UV–Vis Transitions for $[Rh_2(\mu\text{-}EE')(L)_2(\mu\text{-}X)]PF_6$ Complexes.

X	L	EE'	λ_{max}, nm	X	L	EE'	λ_{max}, nm
4B35mpz	CO	dppm	492	345Bpz	CO	dppm	481
	CO	dapm	484		CO	dapm	484
	CO	dpam	473		CO	dpam	462
	t-BuNC	dppm	505		*t*-BuNC	dppm	492
	t-BuNC	dapm	504		*t*-BuNC	dapm	495
	t-BuNC	dpam	493		*t*-BuNC	dpam	480

[a] Values for the lowest energy UV–vis transitions for complexes containing the pz, 4mpz, and the 35mpz complexes are found in ref 6.

Crystal structure analyses have shown that the dpam ligand has a larger bite size than dppm and thus leads to a larger Rh···Rh separation.[5,6] It is reasonable to expect the bite size of the dapm ligand to be between that of dppm and dpam and thus the Rh···Rh separations of the dapm complexes to be between those of the dppm and dpam complexes. As the Rh···Rh separation increases the HOMO will be stabilized since it results mainly from an antibonding combination of metal orbitals. If the LUMO is a ligand antibonding combination, it would be much less affected by changes in the Rh···Rh separation, and the lowest energy electronic transition should move to higher energy as the transoid bridging ligands are changed from dppm to dapm to dpam. This trend is qualitatively illustrated in Figure 3 and was indeed observed in the electronic spectral data previously reported.[6]

The orbital description of Hoffman and co-workers[16] can also be used to explain the trend in $E_{1/2}$ values for the first oxidation process. As the HOMO is stabilized with increasing Rh···Rh separation, the energy required to remove an electron is in the order dppm < dapm < dpam, and thus the $E_{1/2}$ values become more positive in the same order. As the data in Table II reveal, this trend is observed for the dicarbonyl and the diisocyanide complexes.

It is noted from the data in Table II that replacement of the CO with RNC renders the complex more susceptible to oxidation, thus shifting $E_{1/2}$ to less positive values. This behavior might be qualitatively rationalized by using the simple orbital diagram depicted in Figure 4. Consider the dimetal fragment $Rh_2(\mu\text{-}dppm)_2(\mu\text{-}pz)^+$ without the terminal CO or RNC ligands. If the HOMO of this fragment is an antibonding metal combination as previously suggested,[16] the relative energy of this orbital after addition of the CO and RNC ligands will depend on the bonding properties of these ligands. The antibonding orbitals of the CO and RNC ligands form combinations with the appropriate symmetry to overlap with the HOMO of the dirhodium fragment. Since CO is considered to be a better π acceptor than RNC (R = $(CH_3)_3C$), its acceptor orbitals are lower in energy and closer to the HOMO of the dirhodium fragment than those of the RNC ligand and will interact more strongly. This stronger interaction

Table IV. Spectroscopic Data for Dirhodium Paramagnetic Complexes[a]

compd no.	UV-vis λ_{max}, nm (ϵ)	near-IR λ_{max}, nm (ϵ)	IR[b] ν(CN), cm^{-1}	ESR	
				g_{iso}[c]	g_{aniso}
1a	580 (1200), 427 (38 000), 384 (3400) sh	845 (780), 994 (380)	2172, 2161	2.15	2.07, 2.00, 1.99
2a	562 (11 000) 427 (26 000), 384 (3400) sh	849 (630), 990 (310)	2172	2.15	2.06, 2.00, 1.99
3a	583 (1200), 429 (24 700), 386 (3400) sh	862 (850), 996 (370)	2168, 2166	2.16	2.07, 2.00, 1.99
4a	580 (1400), 427 (33 700)	856 (680), 994 (300)	2174, 2156	2.15	2.07, 2.00, 1.99
5a	575 (1900), 421 (29 000), 335 (1950)	846 (750), 988 (375)	2176, 2171	2.16	2.22, 2.19, 2.02
13a	625 (670), 435 (8900)	878 (780), 1039 (440)	2168, 2157		2.06, 2.00, 1.99[e]
14a	620 (800), 433 (9900)	873 (830), 1035 (470)	2170, 2156	*f*	*f*
15a	650 (900), 426 (13 600)	865 (820), 1020 (490)	2174, 2168	2.16	2.06, 2.00, 1.99
23a	610 (1790), 444 (2500)	925 (850), 1190 (340)	2166, 2155		2.06, 2.00, 1.995[e]
24a	605 (445), 436 (940)	915 (240), 1150 (120)	2168, 2156	*f*	*f*
25a	615 (1150), 440 (2500), 394 (1400)	905 (650), 1155 (300)	2172, 2160	2.17	2.06, 2.00, 1.996

[a] The other mixed-valence diisocyanide species were generated in solution but not isolated. [b] All IR spectra contain PF_6^- bands at 839 and 557 cm^{-1}. [c] All isotropic g values were obtained at 25 °C for the α isomer. [d] All anisotropic g values are for the β isomer except in the case of **5a**, and except where noted, all anisotropic g values were recorded from the frozen-solution spectra at −196 °C. [e] The anisotropic g values for **13a** and **23a** were taken from the frozen-solution spectra at −140 °C which also contain frozen-solution signals for the α isomer. [f] ESR spectra were not recorded.

leads to greater stabilization of the HOMO and a greater HOMO–LUMO separation for the CO complex than for the RNC complex. This qualitative description of the bonding is not only consistent with the UV–vis data in Table III and the data previously reported that indicate that the wavelengths of the lowest energy transition are in the order dicarbonyl < carbonyl–isocyanide < diisocyanide for a given pyrazolate ligand,[6] but it is also consistent with the electrochemical data. The diisocyanide complexes exhibit less positive $E_{1/2}$ values (Table II) since they have the higher energy HOMO's and thus are more easily oxidized.

The removal of electrons from the HOMO of the pyrazolato-bridged complexes should result in an increase in the Rh···Rh bond order and a decrease in the Rh···Rh separation since the electron is being removed from a MO formed from the antibonding combination of metal orbitals. The decrease in the Rh···Rh separation should be accompanied by a decrease in the HOMO–LUMO separation for the Rh_2^{3+} complexes. As the data in Table IV indicate, the paramagnetic complexes exhibit weak and broad absorptions in the visible spectrum at wavelengths higher than those observed for the lowest energy transition of the parent compounds. However, the available data are not sufficient to unequivocally assign these transitions since the vacancy left in the HOMO as a result of a one-electron oxidation would allow this level to be the acceptor orbital for transitions that originate from filled lower energy orbitals. These transitions could have energies in this region. Filled orbitals close to the singly occupied HOMO might be expected to lead to transitions with energies in the near-infrared region. Each of the paramagnetic diisocyanide complexes exhibits two absorptions in the near-IR, one in each of the regions 825–925 and 980–1190 nm (Table IV). These near-IR transitions are in the order dppm < dapm < dpam for a given pyrazolate derivative. The parent compounds in which the HOMO is doubly occupied do not exhibit transitions in the near-IR region.

The electrochemical data indicate that the thermodynamic stability of the Rh_2^{3+} complexes increases in the order dpam < dapm < dppm. Thus, it was expected that electron-transfer reactions would occur between the parent Rh_2^{2+} species of a more stable Rh_2^{3+} species and a less stable Rh_2^{3+} species. The electron-transfer reaction (1) and similar reactions between **10a** and **5**, **23a** and **13**, and **23a** and **3** were shown to occur by using UV–vis spectroscopy.

$$\underset{\mathbf{13a}}{[Rh_2(dapm)_2L_2(35mpz)]^{2+}} + \underset{\mathbf{1}}{[Rh_2(dppm)_2L_2(pz)]^{+}} \rightarrow \underset{\mathbf{13}}{[Rh_2(dapm)_2L_2(35mpz)]^{+}} + \underset{\mathbf{1a}}{[Rh_2(dppm)_2L_2(pz)]^{2+}} \quad (1)$$

L = *t*-BuNC

The UV–vis spectra of solutions of **13a** after the addition of various equivalents of **1** are shown in Figure 5. The spectral changes that occur upon adding up to 1 equiv of **1** in multiples of $^1/_4$ equiv are shown in Figure 5a. Spectrum 1 in Figure 5a is that of **13a** and exhibits an absorption maximum at 432 nm.

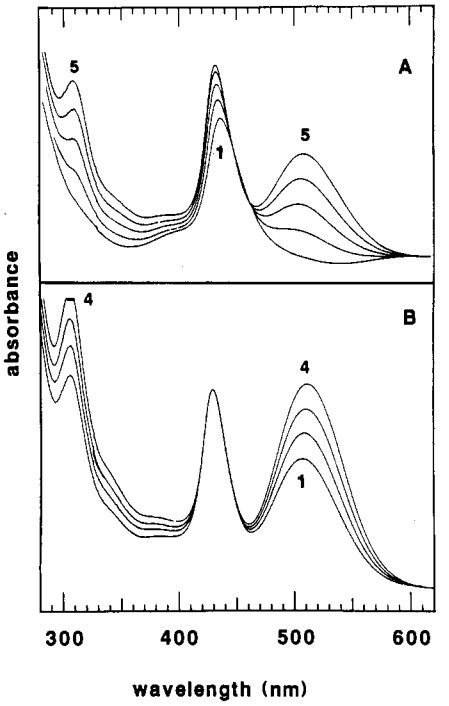

Figure 5. UV–vis spectral changes accompanying the addition of (a) 0–1 equiv or (b) 1–2 equiv of **1** to a CH_2Cl_2 solution of **13a**.

Complex **1a** has an absorption maximum at 427 nm. The absorption profiles observed in the 427–434-nm region for mixtures of **1** and **13a** result from the overlap of the absorption bands of **13a** and **1a**. Since the addition of **1** to **13a** is accompanied by an increase in the amount of **1a** and a decrease in the amount of **13a**, the absorption maximum gradually shifts from 432 to 427 nm. The band increases in intensity because the molar absorptivity of the band in this region is greater for **1a** than for **13a**. Since **13** is also produced during the electron transfer, absorption bands for **13** appear at 504 and 309 nm.

The spectral changes that occur upon the addition of 1–2 equiv of **1** to **13a** in multiples of $^1/_4$ equiv are shown in Figure 5b and are as expected. Results similar to those shown in Figure 5 were obtained for other combinations of Rh_2^{3+} and Rh_2^{2+} species.

Though we have not been able to isolate the Rh_2^{4+} products that are generated via controlled-potential electrolysis of the dirhodium(I) diisocyanide species, when the Rh_2^{4+} species is generated, addition of the Rh_2^{2+} species to the oxidized solution leads to a comproportionation reaction (eq 2).

$$Rh_2^{4+} + Rh_2^{2+} \rightarrow 2Rh_2^{3+} \quad (2)$$

ESR Spectroscopy. Green solutions of the dppm, dapm, and dpam diisocyanide Rh_2^{3+} complexes exhibit room-temperature solution ESR spectra that consist of an isotropic signal with no

observable hyperfine splitting. The isotropic g values are in the range 2.16 ± 0.01 for all of the diisocyanide complexes studied (Table IV).

A frozen 4:1 CH_2Cl_2/toluene solution of **5a** at −196 °C is green, and its ESR spectrum is shown in Figure 6a. This spectrum resembles very closely those recently reported for some other mixed-valence dirhodium complexes.[3,8a-c,10,12] This spectrum is interpreted as that of an orthorhombic system with observable resonances at g values of 2.02, 2.19, and 2.22. The high-field resonance is clearly split into a triplet. This splitting is the result of magnetic interaction of the odd electron with two equivalent ^{103}Rh (100%, $I = {}^1/_2$) nuclei with a hyperfine coupling constant of 20.05×10^{-4} cm^{-1}. These results present clear evidence that the unpaired electron spin is delocalized over the two rhodium atoms. In the case of the related dirhodium complex $[Rh_2(dimen)_2(\mu\text{-dppm})_2](PF_6)_2$ (dimen = 1,8-diisocyanomethane) which also contains two transoid bis(diphenylphosphino)methane ligands,[12] one of the ESR resonances occurs as a five-line pattern for which the splitting is attributed to hyperfine coupling to the four equivalent phosphorus atoms. In this previous report it was noted that an expected third ESR resonance was not observed and was presumed to be masked by the five-line multiplet. In the case of **5a**, a six-line multiplet is observed. If the hyperfine interactions in **5a** along the three magnetic axes are interpreted so as to parallel those assigned to $[Rh_2(dimen)_2(\mu\text{-dppm})_2](PF_6)_2$, the six-line multiplet would be interpreted as the superimposition of the expected third resonance of the orthorhombic system at $g = 2.22$ and a five-line pattern at $g = 2.19$ due to coupling to the four equivalent phosphorus atoms. However, another, and probably more acceptable, interpretation of the data for **5a** is possible. If rhodium hyperfine coupling is occurring along all three magnetic axes, the six-line multiplet is then interpreted as resulting from the splitting of both the low-field and intermediate-field components into triplets.

Unlike the behavior of the CH_2Cl_2/toluene solution of **5a**, solutions of **1a–4a** in 4:1 CH_2Cl_2/toluene change color from green to red upon freezing at −196 °C. This color change does not occur for any of the polycrystalline samples. The red frozen solutions of **1a–4a** exhibit ESR spectra that are quite different from the frozen-solution spectrum of **5a**. The spectra of **1a–4a** are interpreted as those of anisotropic systems for which the high-field and intermediate-field absorptions overlap. Because of this overlap the g values for these absorptions cannot be accurately determined; however, the three g values are essentially the same for the four complexes, 2.06 ± 0.01, 2.00, and 1.99.

It should be noted that the nature of the ESR signals and the g values for **1a–4a** are significantly different from those observed for **5a**. It should also be noted that the low-field ESR absorptions of **1a** and **2a** (Figure 6b,c), with hydrogen atoms in positions 3, 4, and 5 for **1a** and positions 3 and 5 for **2a**, show some unresolved splitting whereas the analogous resonances for **3a** and **4a** (Figure 6d,e), both of which contain methyl groups in positions 4 and 5, are unsplit. These results suggested that the splitting of the low-field signals for **1a** and **2a** might result from hyperfine coupling with the hydrogen atoms on the heterocyclic ring, particularly those in the 3- and 5-positions since substitution here removes the splittings. This interpretation of the data would mean that the odd electron is ligand-based and that an electronic isomerization occurs as the temperature is lowered from room temperature to −196 °C, thus causing the observed reversible thermochromic behavior. It therefore became desirable to investigate the effects of deuterium substitution on the ESR spectra. The literature procedure[17] for preparing the deuteriated pyrazolate ligand gives a product whose mass spectrum clearly identifies it as a mixture of fully and various partially deuteriated ligands. Thus, the dirhodium complex prepared with this product could not unequivocally resolve the question of whether the splitting of the low-field resonances of **1a** and **2a** results from proton hyperfine interaction.

(17) Troitska, V. S.; Konevskaya, N. D.; Vinokurov, V. G.; Tyulin, V. I. *Chem. Heterocycl. Compd.* **1974**, *18*, 2060.

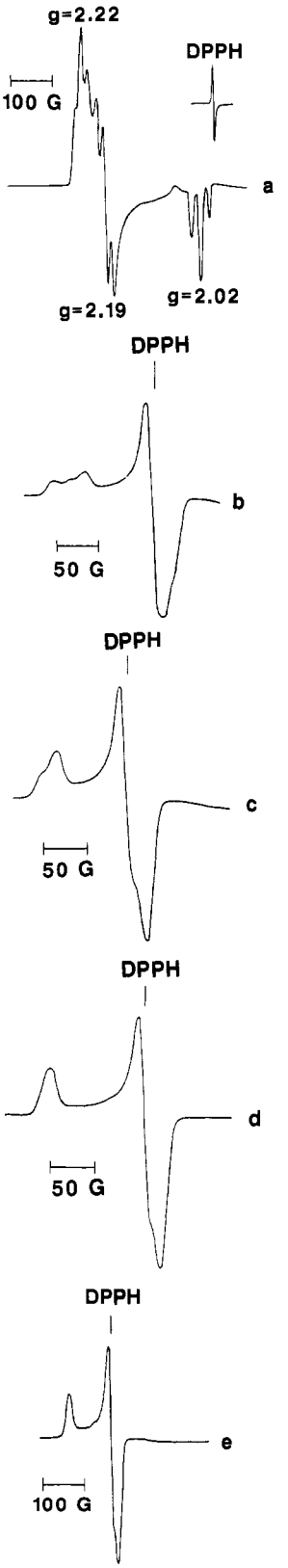

Figure 6. X-Band ESR spectra of 4:1 CH_2Cl_2/toluene solutions at −196 °C of (a) **5a**, (b) **1a**, (c) **2a**, (d) **3a**, and (e) **4a**.

The room-temperature ESR spectrum of a green 4:1 CH_2Cl_2/toluene solution of the dapm complex that contains the 345Bpz ligand, **15**, is shown in Figure 7a. As in the case of **5a** this signal is isotropic with no observable hyperfine splitting. When the temperature is lowered to −120 °C, the solution becomes purple and the ESR spectrum exhibits resonances that indicate the presence of two isomers. The first isomer, which we designate as the α isomer, exhibits an anisotropic spectrum similar to that observed for **5a** at −196 °C (Figure 6a), and the second isomer,

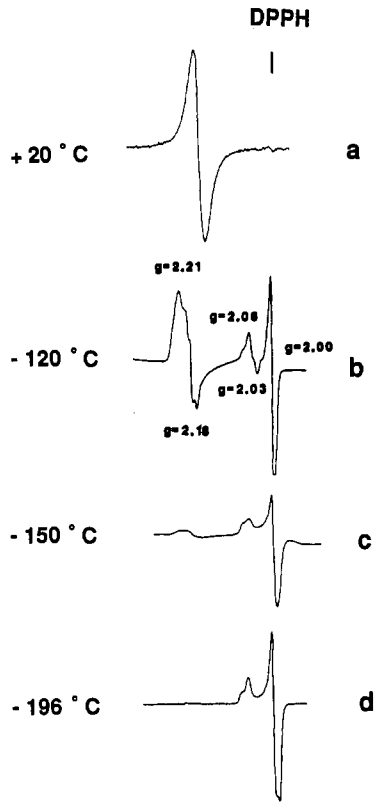

Figure 7. Variable-temperature X-band ESR spectra of a 4:1 CH_2Cl_2/toluene solution of **15a**.

hereafter designated as the β isomer, exhibits an anisotropic spectrum similar to those observed for **1a–4a**. The spectrum of the α isomer consists of three resonances. One resonance occurs at $g = 2.03$ and appears as an unresolved triplet resulting from hyperfine interaction of the odd electron with the two equivalent ^{103}Rh atoms. The second resonance of this isomer occurs at $g = 2.18$ and also appears as a triplet. When the spectrum of **15a** is compared with that of **5a**, this triplet might be attributed to hyperfine interaction ($A = 20.82 \times 10^{-4}$ cm^{-1}) of the odd electron with the two equivalent rhodium atoms; however, this assignment is not unequivocal based on the available data. The third resonance assigned to the α isomer of **15a** occurs at $g = 2.21$ with no observable hyperfine splitting.

The β isomer of **15a** exhibits an resonance near $g = 2.06$ showing unresolved splitting and a strong resonance at $g = 2.00$ which, as in the case of **1a–4a**, is interpreted as resulting from the overlap of two of the three expected resonances in the anisotropic spectrum. It should be mentioned that the ^{31}P NMR spectrum of the parent complex **15** indicates the presence of both a head-to-head (HH) and a head-to-tail (HT) isomer; however, as has been shown to be the case for other dirhodium complexes containing transoid dapm ligands, the head-to-tail (HT) isomer is the more dominant isomer.[18] We do not observe resonances in the ESR spectrum of **15a** that can be attributed to a paramagnetic HH isomer.

Parts c and d of Figure 7 illustrate that at −150 °C only a trace of the α isomer of **15a** remains, though the solution still has a reddish-purple color, and at −196 °C the α isomer has completely disappeared and only the red β isomer remains. The variable-temperature ESR studies of **15a** clearly indicate that the thermochromism is continuous and is the result of isomerization in which the α and β isomers have distinctly different colors.

The dpam complex, **30a**, which also contains the bridging 345Bpz ligand, exhibits a room-temperature ESR spectrum for the 4:1 CH_2Cl_2/toluene solution that consists of a single isotropic signal due to the α isomer at $g = 2.17$. At −120 °C resonances at $g = 2.00$ and 2.06, typical of the low-temperature β isomer, are the only ones observed. This indicates that complete isomerization of the dpam complex occurs at temperatures above −120 °C.

The ESR data of the dppm, dapm, and the dpam complexes **5a**, **15a**, and **25a**, all of which contain the bridging 345Bpz ligand, indicate that if it can be assumed that at some temperature below −196 °C the dppm 345Bpz complex will isomerize to the β isomer, the temperatures at which isomerization occurs are in the order dppm < dapm < dpam. Regardless of whether the isomerization is electronic or structural in nature, it clearly is facilitated, at least in the case of the 345Bpz complexes, by substitution of a As for a P in the transoid bridging ligand.

Other pyrazolato-bridged paramagnetic complexes can also occur as mixtures of the α and β isomers. For example, the ESR spectrum of complex **28a** at −140 °C contains resonances that indicate the presence of both isomers. The variation in g values as the temperature is lowered for the pyrazolato-bridged dirhodium complexes is similar to that observed with a change in concentration for a related triazenido-bridged dirhodium complex.[10]

Paramagnetic dppm dicarbonyl complexes can be generated for the dicarbonyl complexes **6–10**. In CH_2Cl_2/toluene solution these complexes exhibit the expected anisotropic ESR spectra at −196 °C; however, on the basis of the lack of any significant variation in g values with temperature, it is concluded that the α form does not isomerize to the β form down to −196 °C.

Conclusions. The nature of the isomerization of the Rh_2^{3+} pyrazole-bridged complexes that leads to the observed thermochromism is unclear. A thermally induced electronic isomerization, i.e. metal-to-ligand or ligand-to-metal charge transfer, would require a change in the oxidation state of the metal centers. Room-temperature infrared spectroelectrochemistry indicates that the change in ν(NC) in going from the Rh_2^{2+} to the Rh_2^{3+} diisocyanide species is ca. 55 cm^{-1} and from Rh_2^{3+} to Rh_2^{4+} is ca. 17 cm^{-1}. Low-temperature external reflectance infrared spectroscopy indicates that the difference in the ν(NC) stretching frequency between the green α isomer at room temperature and the red β isomer at −196 °C is only about 5–7 cm^{-1}. Such a small change suggests that the metal centers have not undergone a change in oxidation state during the isomerization. Thus, it is likely that the isomerization is structural in nature. Though there are several possible structural distortions that might occur and lead to the isomerization, two rare structural features have been recently observed that might play a role in the isomerization observed here. It has recently been shown that dirhodium complexes containing two bridging dppm ligands in a cis disposition can exist;[19] therefore, a temperature-dependent distortion of the trans dppm-bridged complex toward a cis dppm-bridged species is not unreasonable. Also, we have recently demonstrated by X-ray structure analysis that a dirhodium trans dppm-bridged species can exist in which the methylene moieties of the dppm ligands are folded away from a bridging ligand that is cis to the two dppm ligands.[20] This orientation is the opposite of what other structural analyses have shown to be the favored orientation of the methylene moieties of the dppm ligands. Studies aimed at further elucidation of the nature of the β isomer of the pyrazolato-bridged dppm dirhodium complexes are in progress.

Acknowledgment. We thank the National Science Foundation and the Department of Energy for support of this work and Johnson Matthey, Inc., for a generous loan of rhodium(III) chloride. We also wish to thank Paul Flowers of the Department of Chemistry, University of Tennessee, for his assistance in the design and construction of the cell used in the infrared spectroelectrochemistry experiments and for his assistance in obtaining the infrared spectra.

(18) (a) Enlow, P. D.; Woods, C. *Organometallics*, **1983**, *2*, 64. (b) Guimerans, R. R.; Balch, A. L. *Inorg. Chim. Acta* **1983**, *77*, L177.

(19) Cotton, F. A.; Dunbar, K. R.; Verbruggen, M. G. *J. Am. Chem. Soc.* **1987**, *109*, 5498.

(20) Tortorelli, L. J.; Woods, C. Unpublished results.